Proceedings of the 10th Brazilian Congress of Thermal Sciences and Engineering -- ENCIT 2004
Braz. Soc. of Mechanical Sciences and Engineering -- ABCM, Rio de Janeiro, Brazil, Nov. 29 -- Dec. 03, 2004

Paper CIT04-0204

NUMERICAL MODELING OF SUPERCRITICAL DROPLET-STREAM COMBUSTION

Aldélio Bueno Caldeira
Military Engineering Institute, Mechanical and Materials Engineering Department - 22290-270 - Rio de Janeiro - RJ - Brazil
aldelio@ime.eb.br

Albino José Kalab Leiroz
Federal University of Rio de Janeiro, Mechanical Engineering Program - 21945-970 - Rio de Janeiro - RJ - Brazil
leiroz@ufrj.br

Helcio Rangel Barreto Orlande
Federal University of Rio de Janeiro, Mechanical Engineering Program - 21945-970 - Rio de Janeiro - RJ - Brazil
helcio@serv.com.ufrj.br

Abstract. This work presents the numerical solution for the combustion of an infinite stream of droplets in a stagnant oxidizing environment, under supercritical conditions. The combustion process is considered isobaric and the fluid motion is induced by density gradients due to the heat and mass transfer processes. The model is based on mass, momentum and Shvab-Zel`dovich potential conservation equations and considers the Simple Chemical Reaction mechanism and ideal gas behavior. The thermophysical properties, except the density, are assumed constant. The Finite Volume Method is employed for the numerical solution, using a generalized system of coordinates formulation. A non-staggered grid is used and the SIMPLEC algorithm is employed to solve the modified pressure-velocity coupling. The results for the limiting case of an isolated droplet are compared with benchmark results available in the literature.

Keywords: combustion, droplet, supercritical, diffusion flame

1. Introduction

Supercritical droplet vaporization and combustion is presented in many engineering systems such as Diesel engines, gas turbines, rocket engines and regenerative liquid propellant guns. The supercritical droplet vaporization and combustion refers to conditions in which the droplets surfaces are equal or greater than the critical mixing state throughout droplets lifetime. Droplet vaporization and combustion in supercritical thermodynamic conditions introduces challenges associated with high temperature and pressure conditions and of the absence of surface tension effects. Reviews on supercritical droplet vaporization and combustion indicate the absence of experimental data available (Aggarwal and Yan, 2002). Therefore, the numerical modeling of supercritical droplet combustion becomes an important engineering tool. Besides, within dense sprays, interactive effects are important for a precise description of the phenomena. The droplet-stream is a simple spray arrangement that retains information about the droplet interaction effects. This configuration allows the analysis of the droplet interactions on the flame and droplet shapes, combustion time and energy, momentum and species fields' behavior (Leiroz, 1996, Caldeira, 2004). In supercritical conditions the droplet shape is defined by arbitrated criteria of density, temperature, or species concentration (Bellan, 2000, Daou and Rogg, 1998).

The numerical modeling of an infinite supercritical droplet-stream combustion is shown in this work. The Finite Volume Method is employed for the numerical solution by using a generalized system of coordinates formulation associated with a hybrid mesh generation (Caldeira, 2004). A non-staggered grid is used and the SIMPLEC algorithm is employed to solve the modified pressure-velocity coupling. To validate the numerical model, results for the limiting case of an isolated droplet are compared with benchmark results available in the literature.

2. Physical and mathematical model

The physical model considered here involves the combustion of an infinity stream of supercritical droplets. In the mathematical model the thermo-physical properties are constants, with the exception the density that is assumed as a function of the temperature through the ideal gas law. Furthermore, the system is considered isobaric, the Simple Chemical Reaction System hypothesis is employed and the values of diffusivities of mass and energy are considered equal for each species. The mathematical model is based on the mass, momentum and Shvab-Zel`dovich potential conservation equations and on the ideal gas equation of state (Daou and Rogg, 1998). The fuel droplet-stream, with mono-sized and equidistant droplets, is assumed to be initially inside a pure oxidant environment. Also, the temperature inside the droplet stream is supposed constant and lower than the constant ambient temperature, and the droplets and the

atmosphere are stagnant. It is important to note that in some engineering systems the oxidant may constitute the droplets while the fuel constitutes the atmosphere.

The ideal-gas assumption introduces errors in the supercritical droplet combustion model near critical conditions. Although, it has been reported as a good assumption for supercritical droplet combustion far from the critical conditions or for the case of gas pockets (Sánchez-Tarifa et al., 1972). The Sánchez-Tarifa et al., (1972) statement can be explained from the compressibility factor behavior for conditions well above the critical ones. In such conditions, the value of compressibility factor becomes one. The constant thermo-physical properties, unitary Lewis number and isobaric system simplifying assumptions were also applied by Daou and Rogg (1998). These assumptions are also used in the present work in order to allow for the validation of the developed model and reduce computational costs.

The dimensionless form of the conservation equations of the model is presented in Eq. 1 to Eq. 9. These equations are written in the spherical coordinated system (R,θ) with origin positioned in the center of the droplet, as shown in the Figure 1. In the momentum equations, p is the modified pressure (Daou and Rogg, 1998) where the thermodynamic pressure and the volumetric expansion terms are grouped and Re is the Reynolds number. In the Shvab-Zel`dovich potential conservation equation, Pe is the Peclet number. In the equation of state, $f_{st}$ is the stoichiometric Shvab-Zel`dovich potential, e is the initial ratio of the droplet temperature by the ambient temperature and q is the heat of reaction. The dependent variables of the model are: density (ρ), radial velocity (u), azimuthal velocity (v) and the Shvab-Zel`dovich potential (f).

$$\frac{\partial\left(\mathrm{R}^2\,\sin\theta\,\rho\right)}{\partial \mathrm{t}}+\frac{\partial\left(\mathrm{R}^2\,\sin\theta\,\rho\,\mathrm{u}\right)}{\partial \mathrm{R}}+\frac{\partial\left(\mathrm{R}\,\sin\theta\,\rho\,\mathrm{v}\right)}{\partial\theta}=0 \tag{1}$$

$$\frac{\partial\left(\mathrm{R}^2\,\sin\theta\,\rho\,\mathrm{u}\right)}{\partial \mathrm{t}}+\frac{\partial\left(\mathrm{R}^2\,\sin\theta\,\rho\,\mathrm{u}\,\mathrm{u}\right)}{\partial \mathrm{R}}+\frac{\partial\left(\mathrm{R}\,\sin\theta\,\rho\,\mathrm{v}\,\mathrm{u}\right)}{\partial\theta}-\rho\,\mathrm{v}^2\,\mathrm{R}\,\sin\theta= -\mathrm{R}^2\,\sin\theta\,\frac{\partial \mathrm{p}}{\partial \mathrm{R}}+\frac{\partial}{\partial \mathrm{R}}\left(\mathrm{R}^2\,\sin\theta\,\tau_{\mathrm{RR}}\right)+\frac{\partial}{\partial\theta}\left(\mathrm{R}\,\sin\theta\,\tau_{\mathrm{R}\theta}\right)-\mathrm{R}\sin\theta\left(\tau_{\theta\theta}+\tau_{\varphi\varphi}\right) \tag{2}$$

$$\frac{\partial\left(\mathrm{R}^2\,\sin\theta\,\rho\,\mathrm{v}\right)}{\partial \mathrm{t}}+\frac{\partial\left(\mathrm{R}^2\,\sin\theta\,\rho\,\mathrm{u}\,\mathrm{v}\right)}{\partial \mathrm{R}}+\frac{\partial\left(\mathrm{R}\,\sin\theta\,\rho\,\mathrm{v}\,\mathrm{v}\right)}{\partial\theta}+\rho\,\mathrm{u}\,\mathrm{v}\,\mathrm{R}\,\sin\theta= -\mathrm{R}\,\sin\theta\,\frac{\partial \mathrm{p}}{\partial\theta}+\frac{\partial}{\partial \mathrm{R}}\left(\mathrm{R}^2\,\sin\theta\,\tau_{\mathrm{R}\theta}\right)+\frac{\partial}{\partial\theta}\left(\mathrm{R}\,\sin\theta\,\tau_{\theta\theta}\right)+\mathrm{R}\sin\theta\left(\tau_{\mathrm{R}\theta}-\cot\mathrm{g}\,\theta\,\tau_{\varphi\varphi}\right) \tag{3}$$

$$\tau_{\mathrm{RR}}=\frac{2}{\mathrm{Re}}\frac{\partial \mathrm{u}}{\partial \mathrm{R}} \tag{4}$$

$$\tau_{\theta\theta}=\frac{2}{\mathrm{R}\,\mathrm{Re}}\left(\frac{\partial \mathrm{v}}{\partial\theta}+\mathrm{u}\right) \tag{5}$$

$$\tau_{\varphi\varphi}=\frac{2}{\mathrm{R}\,\mathrm{Re}}\left(\mathrm{u}+\mathrm{v}\,\cot\mathrm{g}\,\theta\right) \tag{6}$$

$$\tau_{\mathrm{R}\theta}=\frac{1}{\mathrm{Re}}\left(\frac{\partial \mathrm{v}}{\partial \mathrm{R}}-\frac{\mathrm{v}}{\mathrm{R}}+\frac{1}{\mathrm{R}}\frac{\partial \mathrm{u}}{\partial\theta}\right) \tag{7}$$

$$\frac{\partial\left(\mathrm{R}^2\,\sin\theta\,\rho\,\mathrm{f}\right)}{\partial \mathrm{t}}+\frac{\partial\left(\mathrm{R}^2\,\sin\theta\,\rho\,\mathrm{u}\,\mathrm{f}\right)}{\partial \mathrm{R}}+\frac{\partial\left(\mathrm{R}\,\sin\theta\,\rho\,\mathrm{v}\,\mathrm{f}\right)}{\partial\theta}=\frac{\partial}{\partial \mathrm{R}}\left(\frac{\mathrm{R}^2\,\sin\theta}{\mathrm{Pe}}\frac{\partial \mathrm{f}}{\partial \mathrm{R}}\right)+\frac{\partial}{\partial\theta}\left(\frac{\sin\theta}{\mathrm{Pe}}\frac{\partial \mathrm{f}}{\partial\theta}\right) \tag{8}$$

$$\rho=\left[1-\left(1-\mathrm{e}\right)\mathrm{f}+\mathrm{q}\,\mathrm{f}\right]^{-1},\ \text{for}\ \mathrm{f}\le \mathrm{f}_{\mathrm{st}}$$

$$\rho=\left[1-\left(1-\mathrm{e}\right)\mathrm{f}+\mathrm{q}\,\mathrm{f}_{\mathrm{st}}\,\frac{\left(1-\mathrm{f}\right)}{\left(1-\mathrm{f}_{\mathrm{st}}\right)}\right]^{-1},\ \text{for}\ \mathrm{f}\ge \mathrm{f}_{\mathrm{st}} \tag{9}$$

The definitions of the dimensionless groups employed in this work are given by Eqs. 10.a-k. In this equation the superscript "+" is associated to dimensional variables or parameters and the symbol "∞" is associated to variables or parameters evaluated in a region far from the droplet stream. In Eq. 10.a u_c^+ is the characteristic velocity of the problem, r and z are the cylindrical coordinates as shown by Figure 1, μ is the dynamic viscosity of the fluid and R_0^+ is the initial radius of the droplet.

$$u_c^+ = \frac{\mu_\infty^+}{\rho_\infty^+ R_0^+} \qquad r = \frac{r^+}{R_0^+} \qquad z = \frac{z^+}{R_0^+} \qquad R = \frac{R^+}{R_0^+} \qquad t = \frac{u_c^+ t^+}{R_0^+} \qquad u = \frac{u^+}{u_c^+} \qquad v = \frac{v^+}{u_c^+}$$

$$\rho = \frac{\rho^+}{\rho_\infty^+} \qquad Re = \frac{\rho_\infty^+ u_c^+ R_0^+}{\mu_\infty^+} \qquad Pe = \frac{\rho_\infty^+ c_{p,\infty}^+ u_c^+ R_0^+}{k_\infty^+} \qquad P = \frac{P^+}{\rho_\infty^+ u_c^+ u_c^+} \tag{10.a-k}$$

The domain is simplified when the symmetries of the problem are considered as can be seen in Figure 1. In this figure, b+ is the half interdroplet distance and c+ is the cylindrical radial truncation position of the domain where the infinity boundary conditions are applied.

In the initial conditions, the velocities are zero and the Shvab-Zel`dovich potential is defined as

$$f = 1, \text{ for } R \le 1$$
$$f = 0, \text{ for } R > 1 \tag{11}$$

Homogeneous flux boundary conditions are applied for the dependant variables along each of the symmetry planes and along the outflow boundary.

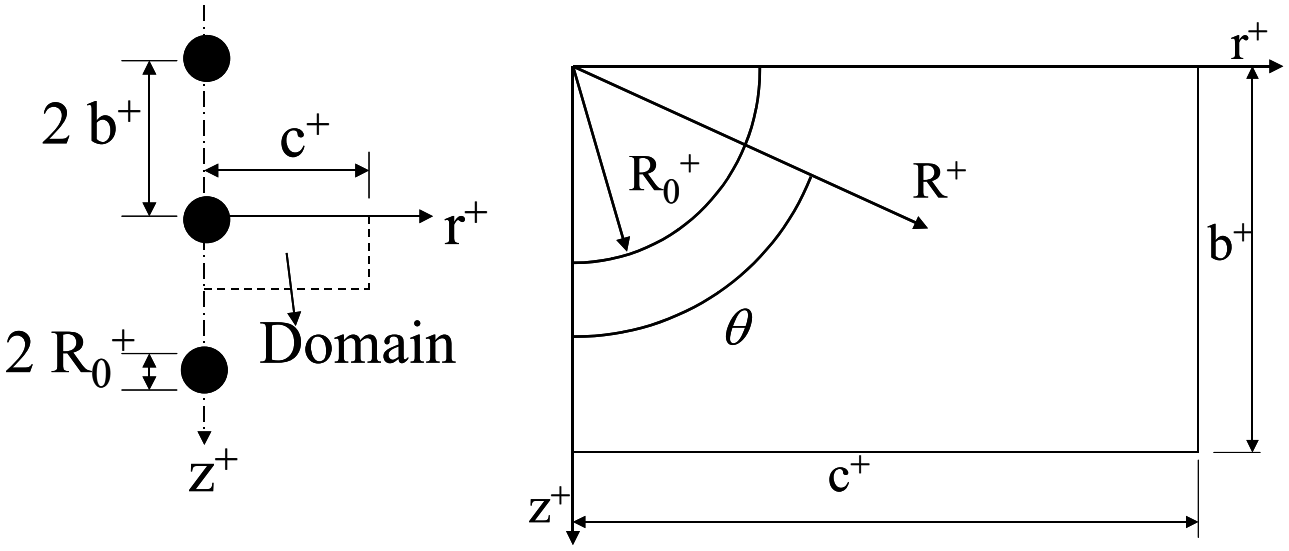

(a) (b)

Figure 1. Physical model: (a) geometry and (b) simplified domain.

3. Numerical solution

The conservation equations presented in Eq. 1 to Eq. 9 are transformed to a generalized coordinated system (ξ,η) as described by Thompson et al. (1985). The finite volume method is employed in a non-staggered grid (Maliska, 1995) and the (modified) pressure-velocity coupling is solved by the SIMPLEC algorithm (Van Dormaal and Raithby, 1984). The WUDS (Raithby and Torrance, 1974) is used as the interpolation function in an implicit scheme. The linear systems of equations are solved by the GMRES algorithm (Press et al. 1992).

Figure 2 presents the qualitative behavior of the numerical-analytical mesh and its regions, which are used in the numerical solution. The hybrid mesh is algebraically generated within the droplet near and far fields. Along the transition region the mesh is numerically generated. The procedure to generate the mesh is split into three steps. In the first step, the region 2 is numerically generated by solving the system of equations given by Eq. 12 and Eq. 13, with second kind boundary conditions at the borders, as given by Eq. 14. These boundary conditions intend to become the mesh approximately orthogonal on the borders of region 2. In the second step, the mesh for region 3 is generated analytically by employing Eq. 21 to Eq. 23. In the third step, the mesh of the region 1 is analytically generated employing Eq. 24 and Eq. 25,

$$\alpha_m \frac{\partial^2 z}{\partial \xi^2} - 2\,\beta_m \frac{\partial^2 z}{\partial \xi\,\partial \eta} + \gamma_m \frac{\partial^2 z}{\partial \eta^2} + J_m{}^2 \left(P \frac{\partial z}{\partial \xi} + Q \frac{\partial z}{\partial \eta} \right) = 0 \tag{12}$$

$$\alpha_m \frac{\partial^2 r}{\partial \xi^2} - 2\,\beta_m \frac{\partial^2 r}{\partial \xi\,\partial \eta} + \gamma_m \frac{\partial^2 r}{\partial \eta^2} + J_m{}^2 \left(P \frac{\partial r}{\partial \xi} + Q \frac{\partial r}{\partial \eta} \right) = 0 \tag{13}$$

$$\frac{\partial r}{\partial \xi}\frac{\partial z}{\partial \eta} + \frac{\partial r}{\partial \eta}\frac{\partial z}{\partial \xi} = 0 \tag{14}$$

The metrics and the attraction functions of the Eq. 12 and Eq. 13 are defined as

$$\alpha_m \equiv \left(\frac{\partial z}{\partial \eta} \right)^2 + \left(\frac{\partial r}{\partial \eta} \right)^2 \tag{15}$$

$$\gamma_m \equiv \left(\frac{\partial z}{\partial \xi} \right)^2 + \left(\frac{\partial r}{\partial \xi} \right)^2 \tag{16}$$

$$\beta_m \equiv \frac{\partial z}{\partial \xi}\frac{\partial z}{\partial \eta} + \frac{\partial r}{\partial \xi}\frac{\partial r}{\partial \eta} \tag{17}$$

$$J_m \equiv \frac{\partial z}{\partial \xi}\frac{\partial r}{\partial \eta} + \frac{\partial r}{\partial \xi}\frac{\partial z}{\partial \eta} \tag{18}$$

$$\begin{aligned} P(\xi,\eta) \equiv & -\sum_{k=1}^{n} a_k \; \mathrm{Sign}(\xi - \xi_k)\, \mathrm{Exp}\left(-c_k \, |\xi - \xi_k|\right) \\ & -\sum_{k=1}^{m} b_k \; \mathrm{Sign}(\xi - \xi_k)\, \mathrm{Exp}\left(-d_k \, \sqrt{(\xi - \xi_k)^2 + (\eta - \eta_k)^2}\right) \end{aligned} \tag{19}$$

$$\begin{aligned} Q(\xi,\eta) \equiv & -\sum_{k=1}^{n'} A_k \; \mathrm{Sign}(\eta - \eta_k)\, \mathrm{Exp}\left(-C_k \, |\eta - \eta_k|\right) \\ & -\sum_{k=1}^{m'} B_k \; \mathrm{Sign}(\eta - \eta_k)\, \mathrm{Exp}\left(-D_k \, \sqrt{(\xi - \xi_k)^2 + (\eta - \eta_k)^2}\right) \end{aligned} \tag{20}$$

The system of equations written in Eq. 12 to Eq. 14 is numerically solved using the finite differences method and the resulting algebraic linear systems are solved by the algorithm of the Gauss-Seidel with SOR.
For the second step, the points on the border between regions 2 and 3 of the mesh are known. Lines are generated in the cylindrical radial direction from those points up to the truncation boundary of the domain. On these lines, the mesh points are generated with Eqs. (21-23). In these equations, a is the value of r on the frontier between regions 2 and 3, N is the number of points in the direction ξ and ξc is the value of ξ on the border between the regions 2 and 3.

$$\kappa = \frac{\ln\left(\dfrac{c - a}{r_{(\xi_C, M)} - r_{(\xi_C - 1, M)}} \right)}{\ln(N - \xi_C)} \tag{21}$$

$$z_{(\xi,\eta)} = z_{(\xi_c,\eta)} \tag{22}$$

$$r_{(\xi,\eta)} = (c - a)\left(\frac{\xi - \xi_C}{N - \xi_C} \right)^{\kappa} + r_{(\xi_c,\eta)} \tag{23}$$

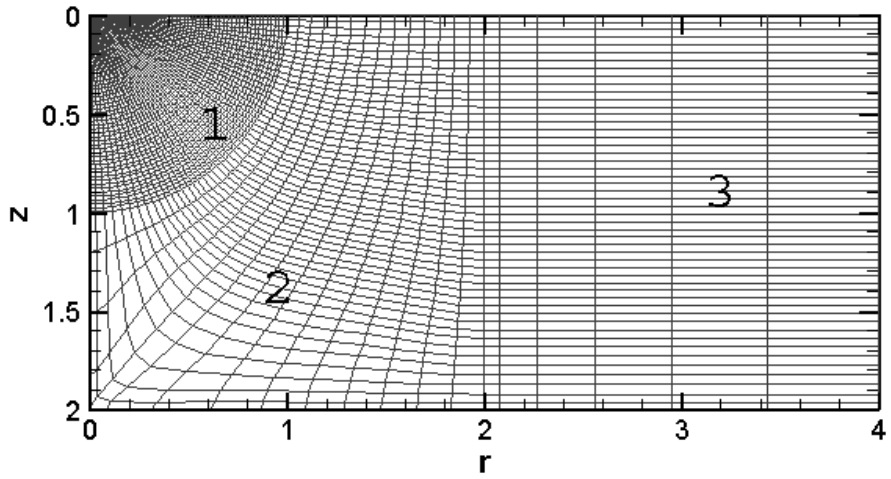

Figure 2. A typical hybrid mesh in the physical plane.

In the third step, the points of the border between regions 1 and 2 are known. Lines are generated in the spherical radial direction from those points to the origin of the spherical coordinated system. On these lines the mesh points are generated with Eqs. (24-27). These equations control the point distribution in three sub-regions limited by the radial spherical positions R_1, R_2 and R_3. However, depending on the case studied, only one, two or three of these sub-regions can be employed to build the spherical region. In Eq. 24 to Eq. 27 $\xi_{(R_1)}, \xi_{(R_2)}$ and $\xi_{(R_3)}$ are the values of ξ corresponding to R_1, R_2 and R_3, respectively, and y_1 and y_3 are arbitrated constants. Furthermore, the border between regions 1 and 2 is not necessarily associated with the initial droplet surface.

$$R(\xi) = R_1 \left(\frac{\xi - 1}{\xi_{(R_1)} - 1} \right)^{y_1}, \qquad \text{in } 0 \geq R \geq R_1 \tag{24}$$

$$R(\xi) = (R_2 - R_1) \left(\frac{\xi - \xi_{(R_1)}}{\xi_{(R_2)} - \xi_{(R_1)}} \right) + R_1, \quad \text{in } R_1 \geq R \geq R_2 \tag{25}$$

$$R(\xi) = (R_3 - R_2) \left(\frac{\xi - \xi_{(R_2)}}{\xi_{(R_3)} - \xi_{(R_2)}} \right)^{y_3} + R_2, \text{ in } R_2 \geq R \geq R_3 \tag{26}$$

$$\theta(\xi, \eta) = \theta(\xi_{(R_3)}, \eta) \tag{27}$$

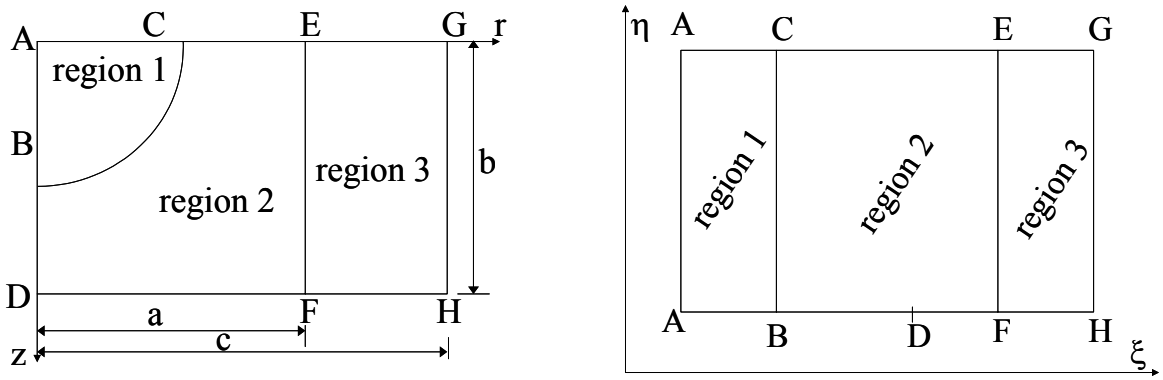

(a) (b)

Figure 3. Regions of the mesh in the physical plane (a) and in the computational plane (b).

Figure 3 shows the regions of the mesh in the physical and in the regular computational domains. The points of the mesh in regions 2 and 3 are in the cylindrical system of coordinates and the points of the mesh in the region 1 are in the spherical system of coordinates. However, all of the points of the mesh must be described in the spherical system of coordinates to be linked in the generalized system of coordinates. This transformation from the cylindrical to the spherical domains was algebraically performed.

The generated mesh uses the procedure developed by Moreira Filho et al. (2002) where the points represent the volumes and their faces. This procedure intends to improve the precision of the metrics.

4. Results

The following results are devoted to the limiting case of supercritical droplet stream combustion with infinity interdroplet distance that corresponds to the case of isolated supercritical droplet combustion. In this case, the mesh generation is simplified, and only region 1 is utilized. The mesh with 160 x 20 volumes used in this work is presented in Figure 4. The limiting case just described is important to analyze the numerical solution behavior and to be compared with the results of Daou and Rogg (1998).

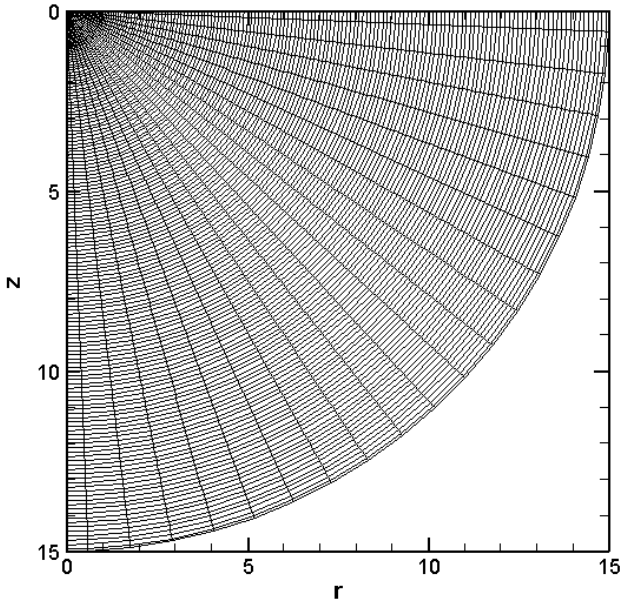

Figura 4 – Algebraic mesh to isolated droplet combustion.

The parameters of the model studied in this work for this case are e = 0.1, b $\rightarrow \infty$, Pe = 1, f_{st} = 0.8 and q = 0 in the case with no heat release and q = 2 in the case with heat release. These parameters and the employed initial conditions for the Shvab-Zel`dovich potential are the same as the ones used by Daou and Rogg (1998), except for the parameter b which is the dimensionless half interdroplet distance present only in the droplet-stream problem ($b = b^+/R_0^+$).

The work of Daou and Rogg (1998) is devoted to the combustion of one supercritical fuel droplet moving in an oxidizing atmosphere. So, the results of Daou and Rogg (1998) for low Reynolds number (Re = 0.1) are compared here with the results reached with the present model that consider the stagnant system as the initial condition.

To make the analysis of the results simpler, some definition are now presented, including the fuel mass

$$FM(t) = \iint_{Vst} \left\{ \left(\frac{f - f_{st}}{1 - f_{st}} \right) \rho \, J \, R^2 \, \sin\theta \right\} d\xi \, d\eta \tag{28}$$

and the normalized fuel mass.

$$NFM(t) = \frac{FM(t)}{FM(0)} \tag{29}$$

In Eq. 28 V_{st} is the volume limited by the isopotential surface f_{st}.

The numerical solution is stopped when the fuel mass in the system is 0.1% of the initial mass of fuel. However, this criterion can fail in cases with heat release. The flame with heat release induces strong velocities gradients in the

vicinity of the flame. At the end of the combustion process the flame goes toward the droplet center that is a stagnation point. This phenomenon can result in numerical convergence problems. To overcome these numerical problems the solution was stopped when the fuel mass in the system was 2.5% of the initial mass of fuel. Nevertheless, the proposed flame model fails at the end of the combustion process, because the model does not consider the extinction of the reaction. Figures 5 and 6 show curves of the mass of fuel present in the domain along time, obtained in the present work and by Daou and Rogg (1998). Figure 5 is related to the case without heat release and Figure 6 is related to the case with heat release.

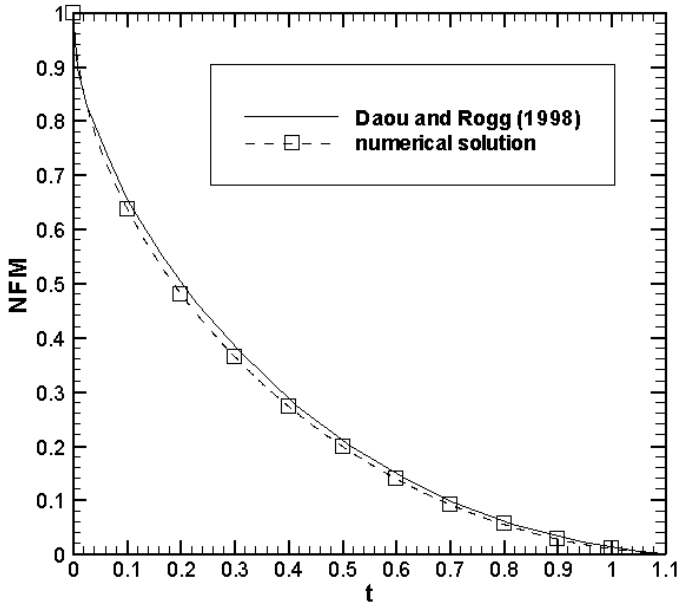

Figure 5. Evolution of the normalized fuel mass along of the time (q = 0). Daou and Rogg, 1998 (solid line), present numerical solution (dashed line)

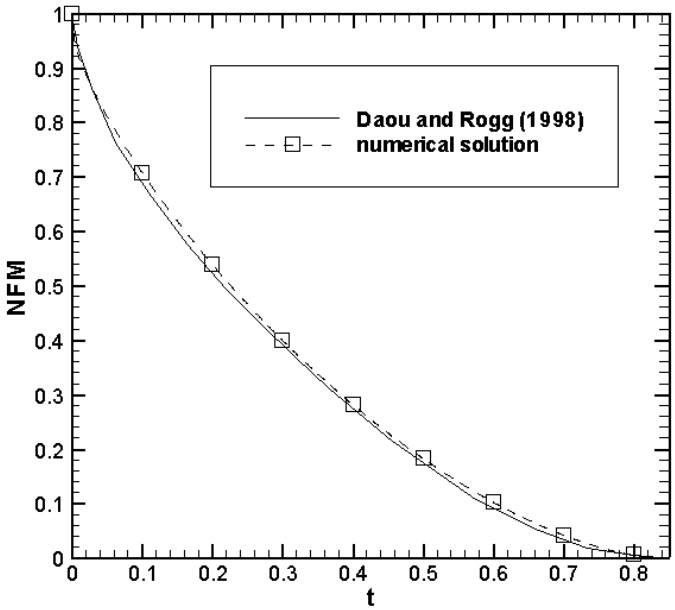

Figure 6. Evolution of the normalized fuel mass along of the time (q = 2). Daou and Rogg, 1998 (solid line), present numerical solution (dashed line)

The maximum absolute discrepancy between the results shown in Figures 5 and 6 are smaller than 0.01. Furthermore, the total time of the combustion process is greater in the case without heat release than in the case with heat release. So, the species transport in the case with q = 2 is more efficient than in the case with q = 0. This is due to the high temperature and low density in the vicinity of the flame for the case with q = 2. The temperature gradient pushes the species into the reaction zone.

In Figure 7 the average radius of the flame (R_f) computed by Daou and Rogg (1998) and the computed flame position in the present work r_{st} and z_{st} on the cylindrical coordinates axis r and z are compared.

An examination of Figure 7 reveals that the r_{st} and z_{st} curves are coincident, indicating the spherical shape of the flame. This shape is physically explained by the angular spherical symmetry of the problem. Furthermore, the

maximum relative discrepancy between the curves in the Figure 7 is smaller than 2.5%. It is important to note that in the proposed model the flame and droplet can change the shape along of the combustion process.

The differences between the results obtained from the proposed model and the one presented by Daou and Rogg (1998) can be attributed to the forced convection, which was not considered in the present work. In fact the forced convection effect pushes the flame against the front of the droplet. However, the average radius evolution shown in Figure 7 reveals that for low Reynolds number, the forced convective effect is more significant in front of the droplet.

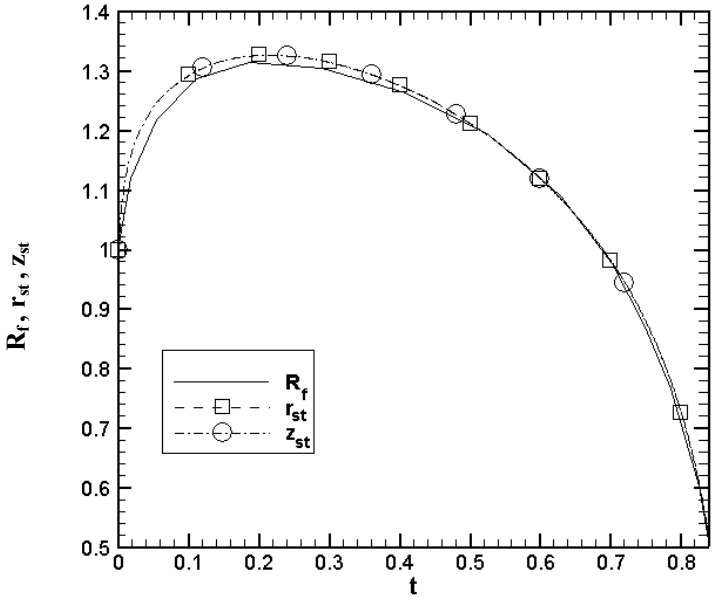

Figure 7. Position of the flame along of the time (q = 2).

The spherical radial profiles for the supercritical isolated droplet combustion, considering parameters described above for the heat release case, are shown in Figure 8. In these conditions the spherical symmetry of the velocity and temperature ($T = 1/\rho$) fields are verified and these profiles are independent of θ. So, the value $\theta = 0.8$ rad is employed to build the curves in Figure 8.

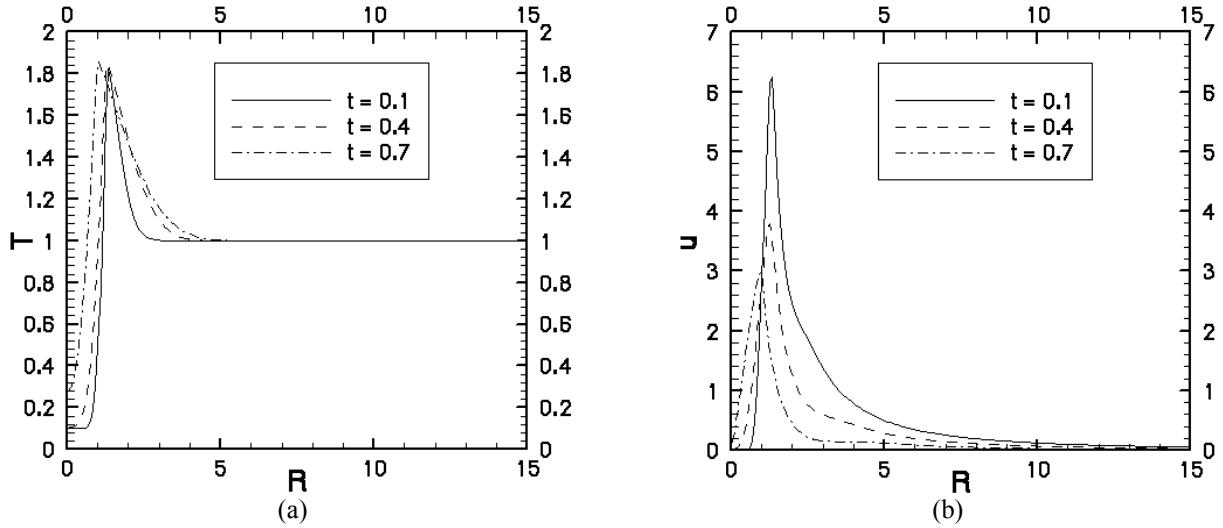

(a) (b)

Figure 8 – Spherical radial velocity and temperature profiles for supercritical isolated droplet combustion (q = 2).

In Figure 8a the evolution of the temperature along of time is represented. In this figure it is possible to note that the maximum temperature takes place at the flame position. Furthermore, the temperature in the center region of the droplet increases with time and the thermal perturbed region by the heat release becomes thicker as time passes. The flame movement in the droplet center direction can be observed in Figure 8a.

Figure 8b shows the evolution of the spherical radial velocity along of time. Observing Figures 8a and 8b it is verified that there is a relationship between the maximum values of temperature and velocity associated with the flame position. In Figure 8b it is possible to note that the velocity gradient increases with time in vicinity of the droplet center.

In Figures 9 and 10 the results obtained with the algebraic mesh of Figure 4 and with the hybrid mesh with 140 x 50 volumes are compared. These solutions consider the reactive case just described in the present work with $b \rightarrow \infty$ for the algebraic mesh case and with b = 8 for the hybrid mesh case.

The results in Figure 9 show that the normalized fuel mass behavior along of the time is, within the graphic scale, the same in both cases. So, the droplet interaction effect, in the hybrid mesh case presented in Figure 9, is not relevant in the droplet-stream combustion with interdroplet distance b = 8. In this situation, the fuel consumption along of time can be considered the same in the isolated droplet case and in the droplet-stream case with b = 8.

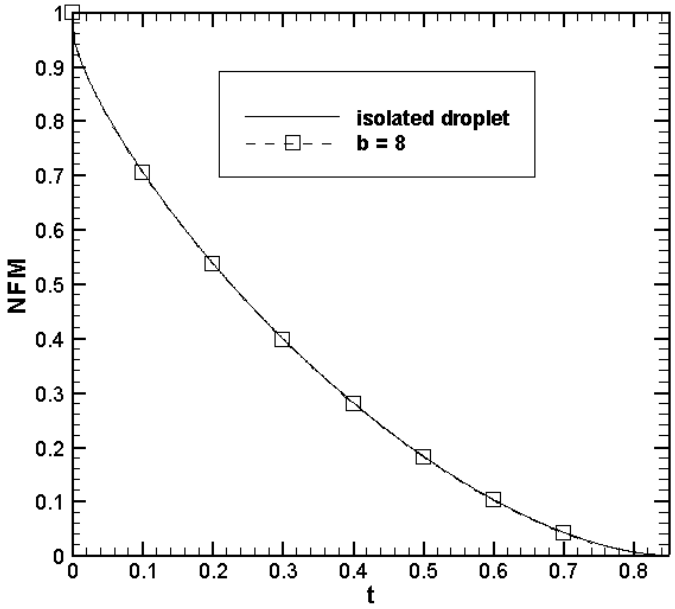

Figure 9. Evolution of the normalized fuel mass along of the time (q = 2).

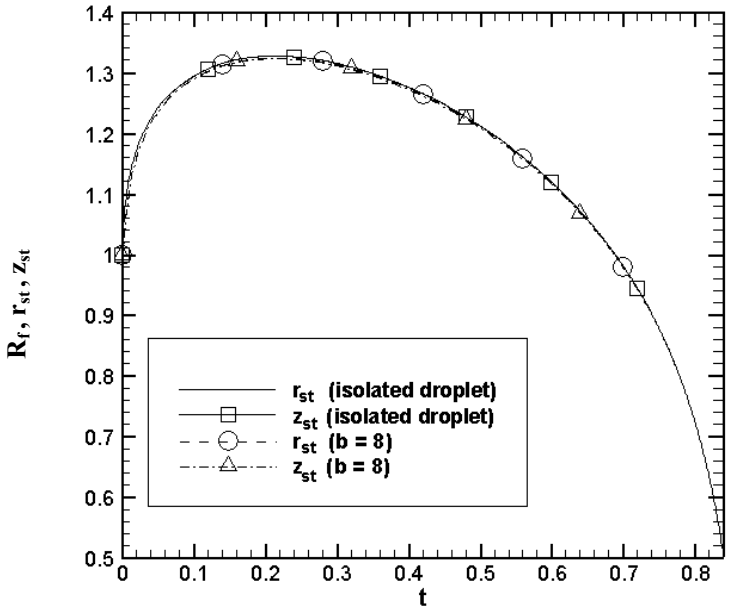

Figure 10. Position of the flame along of the time (q = 2).

In Figure 10, the results of flame position r_{st} and z_{st} on the cylindrical coordinates axis r and z are shown for the cases presented in the Figure 9. The symmetry of the flame shape can be observed in both cases in Figure 10, because the evolution of the flame on the cylindrical coordinates are approximately equal. Furthermore, the droplet interaction effect on the flame behavior is not relevant in the cases studied in the Figure 10.

5. Conclusions

The isolated supercritical droplet combustion case studied in the present work is physically important to represent the supercritical droplet stream combustion with negligible droplet interaction and it is mathematically important to validate the proposed model and numerical method of solution.

The results presented in this work shows that the numerical solution is consistent with the reference results, indicating that the model can be applied to the supercritical droplet combustion problem in stagnant conditions.

The results obtained with the algebraic mesh to the isolated droplet and the ones obtained with the hybrid mesh to the infinity droplet-stream with b = 8 are coincident, indicating that the droplet interaction is not relevant in the studied case. Furthermore, these results show the capability of the hybrid mesh in reproducing the non-interactive droplet results.

6. References

Aggarwal, S. K., Yan, C., 2002, "Transcritical Vaporization of Liquid Fuel Droplet in a Supercritical Ambient", Combustion Science and Technology, v. 174, pp. 103-130.

Bellan, J., 2000, "Supercritical (and Subcritical) Fluid Behavior and Modelling: Drops, Steams, Shear and Mixing Layers, Jets and Sprays", Progress in energy and Combustion Science, v. 26, pp. 329-366.

Caldeira, A. B., 2004, Combustão de uma Coluna de Gotas em Condições Supercríticas, D.Sc. dissertação, Universidade Federal do Rio de Janeiro, Rio de Janeiro, Rio de Janeiro, Brasil.

Daou, J., Rogg, B., 1998, "Convective Burning of Gasous Fuel Pockets and Supercritical Droplets", Combustion and Flame, v. 115, pp. 145-157.

Leiroz, A. J. K., 1996, Numerical Study of Droplet-Stream Vaporization and Combustion, Ph.D. dissertação, University of California at Irvine, Irvine, California, USA.

Maliska, C. R., 1995, Transferência de Calor e Mecânica dos Fluidos Computacional, LTC.

Moreira Filho, E. G., Mejias, M. M., Orlande, H. R. B., Leiroz, A. J. K., 2002, "Computational Aspects of Metrics Evaluation for the Finite Volume Method", In: Proceedings of IX Congresso Brasileiro de Engenharia e Ciências Térmicas, CD ROM, Caxambú.

Press, W. H., Teukolsky, S. A., Vetterling, W. T., Flannery, B. P., 1992, Numerical Recipes in Fortran – The Art of Scientific Computing, 2 ed, Cambridge.

Raithby, G. D., Torrance, K. E., 1974, "Upstream-Weighted Differencing Schemes and Their Application to Elliptic Problems Involving Fluid Flow", Computers & Fluids, v. 2, pp.191-206.

Sánchez-Tarifa, C., Crespo, A., Fraga, E., 1972, "A Theoretical Model for the Combustion of Droplets in Super-critical Conditions and Gas Pockets", *Astronautica Acta*, v. 17, pp. 685-692.

Thompson, J. F., Warsi, Z. U. A., Mastin, C. W., 1985, Numerical Grid Generation – Foundations and Applications, Elsevier Science Publishing.

Van Dormaal, J. P., Raithby, G. D., 1984, "Enhancements of the Simple Method for Predicting Incompressible Fluid Flows", Numerical Heat Transfer B, v. 7, pp. 147-163.